International Journal of
Molecular Sciences

MDPI

Article

Unveiling the Impact of Drug-Sensitive Mutations on HIV-1 Protease Dynamics: A Molecular Dynamics Simulation Study of the T12A, L63Q, and H69N Variants

Haythem Srihi [1], Nabil Abid [2,3], Lavinia Fabeni [4], Caterina Precone [5], Hélène Déméné [6] and Giovanni Chillemi [7,8,*]

1 Research Unit UR17ES30 "Genomics, Biotechnology and Antiviral Strategies", High Institute of Biotechnology of Monastir, University of Monastir, Tahar Hadded Avenue, PB 74, Monastir 5000, Tunisia; srihi.haythem@gmail.com
2 High Institute of Biotechnology of Monastir, Department of Molecular and Cellular Biology, University of Monastir, Tahar Hadded Avenue, BP 74, Monastir 5000, Tunisia; nabilabidbensalem.2014@yahoo.fr
3 Laboratory of Transmissible Diseases and Biological Active Substances LR99ES27, Faculty of Pharmacy, University of Monastir, Rue Ibn Sina, Monastir 5000, Tunisia
4 Laboratory of Virology, National Institute for Infectious Diseases Lazzaro Spallanzani—IRCCS, Via Portuense, 292, 00149 Rome, Italy; lavinia.fabeni@inmi.it
5 Department for Innovation in Biological, Agro-Food and Forest Systems—DIBAF, University of Tuscia, 01100 Viterbo, Italy; caterina.precone@unitus.it
6 Centre de Biochimie Structurale (CBS), INSERM, CNRS, Université de Montpellier, 29 Rue de Navacelles, 34090 Montpellier, France
7 Bioinformatics Research Unit in Infectious Diseases, National Institute for Infectious Diseases Lazzaro Spallanzani—IRCCS, Via Portuense, 292, 00149 Rome, Italy
8 Department of Experimental Medicine, University of Rome "Tor Vergata", Via Montpellier 1, 00133 Rome, Italy
* Correspondence: giovanni.chillemi@inmi.it

Abstract

HIV-1 protease (PR) is an essential enzyme in the viral life cycle and a primary target of antiretroviral therapies, particularly protease inhibitors (PIs). Understanding the dynamics of viral evolution and the factors governing the emergence or loss of resistance-associated mutations is critical for improving PI efficacy and managing drug resistance in HIV/AIDS treatment. In this study, we investigated the impact of three natural HIV-1 polymorphisms (T12A, L63Q, and H69N), whose prevalence varies depending on treatment status and viral subtype, on the structural stability and conformational dynamics of PR using molecular dynamics (MD) simulations. Three independent 500 ns MD simulations were performed for the native protease and each mutant system. Although none of the mutations disrupts the overall structural integrity of HIV-1 PR, they induce mutation-specific alterations in flexibility and residue interactions. In particular, T12A and H69N exhibit increased structural deviations, especially in the flap regions, along with enhanced conformational fluctuations. In contrast, the L63Q mutation shows a slight reduction in flap flexibility compared to both the native protease and the other mutants. Consistently, the fraction of time spent in open-flap conformations is higher for T12A and H69N and lower for L63Q relative to the native system. Moreover, mutations in the Fulcrum (T12A) and Cantilever (L63Q and H69N) regions do not disrupt the long-range network of correlated motions observed in the native protease, both inter- and intra-monomer, but instead increase the extent of correlated and anti-correlated motions in other regions of PR.

Keywords: HIV-1 protease; protease inhibitors; long range protein conformation; molecular dynamics simulations

Academic Editor: Roberta Galeazzi

Received: 28 March 2026
Revised: 20 April 2026
Accepted: 22 April 2026
Published: 25 April 2026

1. Introduction

The evolution of the HIV-1 genome and the emergence of drug-resistant viral variants remain major challenges for the scientific community. HIV resistance is defined as the virus's ability to replicate in the presence of one or more inhibitory molecules. This resistance can be attributed to the error-prone nature of HIV-1 reverse transcriptase (RT), which induces several mutations during virus replication, leading to drug-resistant properties [1].

To date, several classes of antiretroviral drugs are used in the treatment of HIV infection. Each class targets different stages of the HIV life cycle, including virus entry and fusion with the host cell, as well as viral enzymes like protease, reverse transcriptase, and integrase. Currently combination antiretroviral therapy, which includes nucleoside and non-nucleoside RT inhibitors, as well as entry, integrase, in addition to protease inhibitors (PIs), has significantly reduced viral load and improved the life expectancy of people living with HIV (PLH) [2,3]. Indeed, HIV protease (PR) is a crucial drug target for HIV/Acquired Immuno Deficiency Syndrome (AIDS) therapy, and PIs have significantly improved patient outcomes since their introduction in 1995 [4]. HIV-1 PR plays an essential role in viral maturation by processing specific cleavage sites in the Gag and Gag-Pol precursor polyproteins to release mature proteins. This protease-catalyzed processing is essential for forming infectious virus particles [5–7]. The structures and activities of PR, along with its drug-resistant variants and their interactions with inhibitors, have been studied extensively to address the challenges of AIDS antiviral therapy and the evolution of HIV drug resistance [8–13].

Despite the success of combination antiretroviral therapy, the persistence of viral reservoirs and the continuous emergence of resistant variants remain major obstacles to long-term viral suppression [8,10]. In this context, structural and dynamical investigations of HIV-1 protease are crucial not only for understanding resistance mechanisms but also for guiding the design of next-generation inhibitors with improved robustness against mutational escape.

Several terminologies were used to describe the topology of HIV protease according to some mechanistic hypothesis. In this article we adopted the one introduced by De Fabritiis' group [14]. The dimer interface is formed principally from an interdigitated four-stranded beta-sheet (residues 1–5, 96–99) and the so-called fireman's grip (residues 24–29) that provide the base for the active site and entails the catalytic Asp dyad (D25). The active site is enclosed on top by flexible β-hairpin structure called the "flap" (residues 43–58) and laterally by the "wall" (residues 80–83). Additional features of each monomer are the flap elbows (residues 37–42), the cantilever (residues 59–75), the fulcrum (residues 10–23), and the α-helix (residues 87–95) (Figure 1). It was shown that the PR dimer adopts a closed conformation when bound to a substrate or inhibitor, whereas flap opening modulates the entry or release of the ligands [15].

PI-resistance mutations are associated with the highest levels of phenotypic resistance and/or the strongest clinical evidence for interfering with successful PI therapy (https://hivdb.stanford.edu/dr-summary/resistance-notes/PI/, access date on 23 January 2026). It has been reported that three PR mutations located in the fulcrum (T12) and cantilever domains (L63 and H69) [16–18] are categorized as polymorphisms—mutations usually observed more frequently in drug-naïve individuals and typically reduced in prevalence among patients treated with protease inhibitors (PIs) [18,19]. These mutations, although naturally occurring, tend to be negatively selected in PI-treated patients, suggesting a potential compensatory or modulating role. Epidemiological data from the Stanford HIV Drug Resistance Database indicates that T12A, L63Q, and H69N are not primary resistance mutations but may influence protease dynamics and drug susceptibility indirectly. Their prevalence varies depending on treatment status and viral subtype, and they may transiently emerge or disappear under drug pressure, even if the exact role of these mutations

in protease structure has not yet been precisely clarified. To this end, molecular dynamics (MD) simulations were used to simulate protein movements at atomic resolution for the three discussed mutants as well as the native form of HIV protease protein, in three replicas. The resulting structural data were analyzed to investigate the effects of these mutations on protein structure, dynamics, and its ability to function properly.

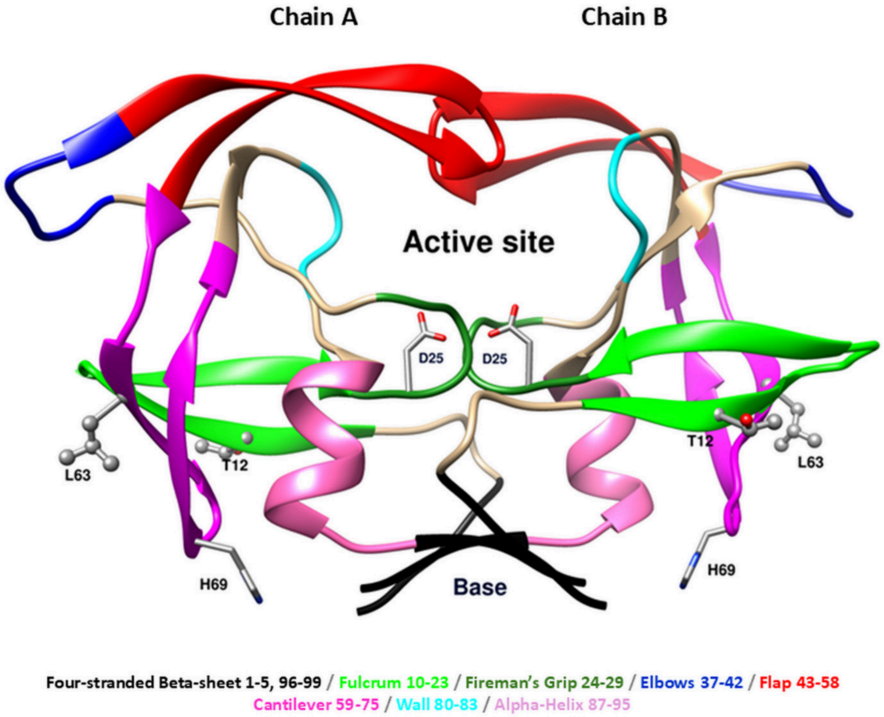

Figure 1. Topology of the HIV-1 protease (PDB ID: 1ODW) in dimeric form. Topology of HIV-1 protease colored according to the convention proposed previously (Sadiq and De Fabritiis, 2010) [14]. The three mutated residues T12, L63, and H69 are shown in ball and stick representation. The catalytic residue D25 is shown in stick representation.

2. Results

2.1. Stability of the HIV-1 PR Systems

Our study first tested the equilibrium state and overall stability of the different protein structures in their apo state along the generated trajectories, using the root-mean-square deviation (RMSD) analysis. All simulations were initiated from energy-minimized closed conformations and simulated for 500 ns.

The average RMSD values and corresponding shaded error ranges, calculated from the three replicas, are shown in Figure 2 for the four systems. The three replicas of the wild-type (WT) exhibit good reproducibility, whereas greater variability is observed among the mutant replicas. Individual RMSD profiles for each replica are reported in Supplementary Figure S1. All systems sample conformations with RMSD values greater than 0.7 nm relative to the initial MD structure. Average, standard deviation and maximum RMSD values for R1, R2 and R3 across all systems are reported in Table 1.

The T12A mutant exhibits higher RMSD values than all other PR systems. However, all mutations lead to increased RMSD values across replicas, indicating an intrinsic effect on the conformational space sampled by PR.

To determine whether these deviations are associated with flap opening, RMSD values were recalculated excluding the flap residues (region 43–58). The resulting average RMSD value and shaded error ranges are shown in Figure 3, while individual replica profiles are provided in Supplementary Figure S2.

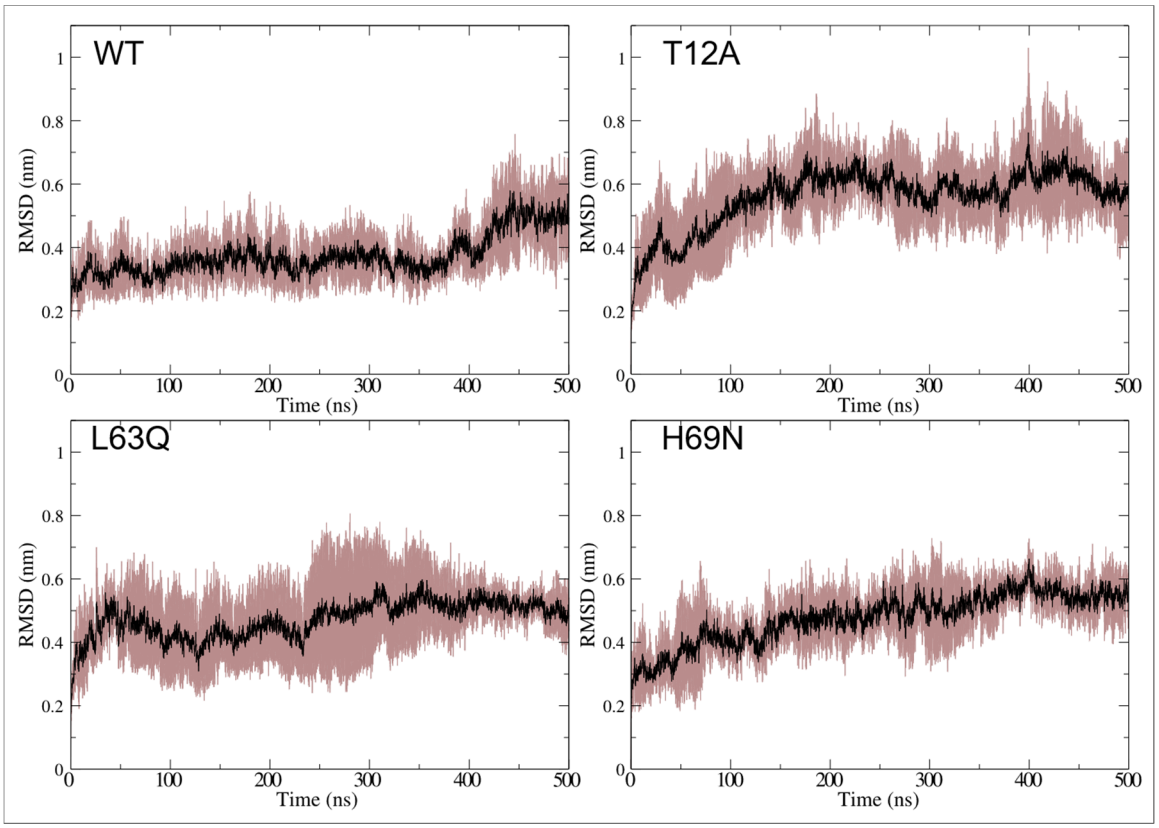

Figure 2. Plot of RMSD of c-alpha atoms, as a function of simulation time for the four simulated PR systems. Average and shaded error range, calculated from the three replicas, are colored in black and brown, respectively.

Table 1. Average and standard deviations RMSD for native and mutated PR (nm) in the 50–500 ns time window.

		All C-Alpha		
		Ave	**St Dev**	**Max**
Native	R1	0.38	0.051	0.59
	R2	0.36	0.096	0.70
	R3	0.40	0.086	0.75
T12A	R1	0.55	0.051	0.72
	R2	0.62	0.140	1.07
	R3	0.57	0.080	0.78
L63Q	R1	0.45	0.06	0.67
	R2	0.58	0.08	0.84
	R3	0.40	0.09	0.61
H69N	R1	0.51	0.10	0.70
	R2	0.52	0.06	0.71
	R3	0.46	0.08	0.73

Average, standard deviation and maximum RMSD values are reported in Table 2, along with the percentage difference between total and "no-flap" RMSD values (see Δ (%) column in Table 2).

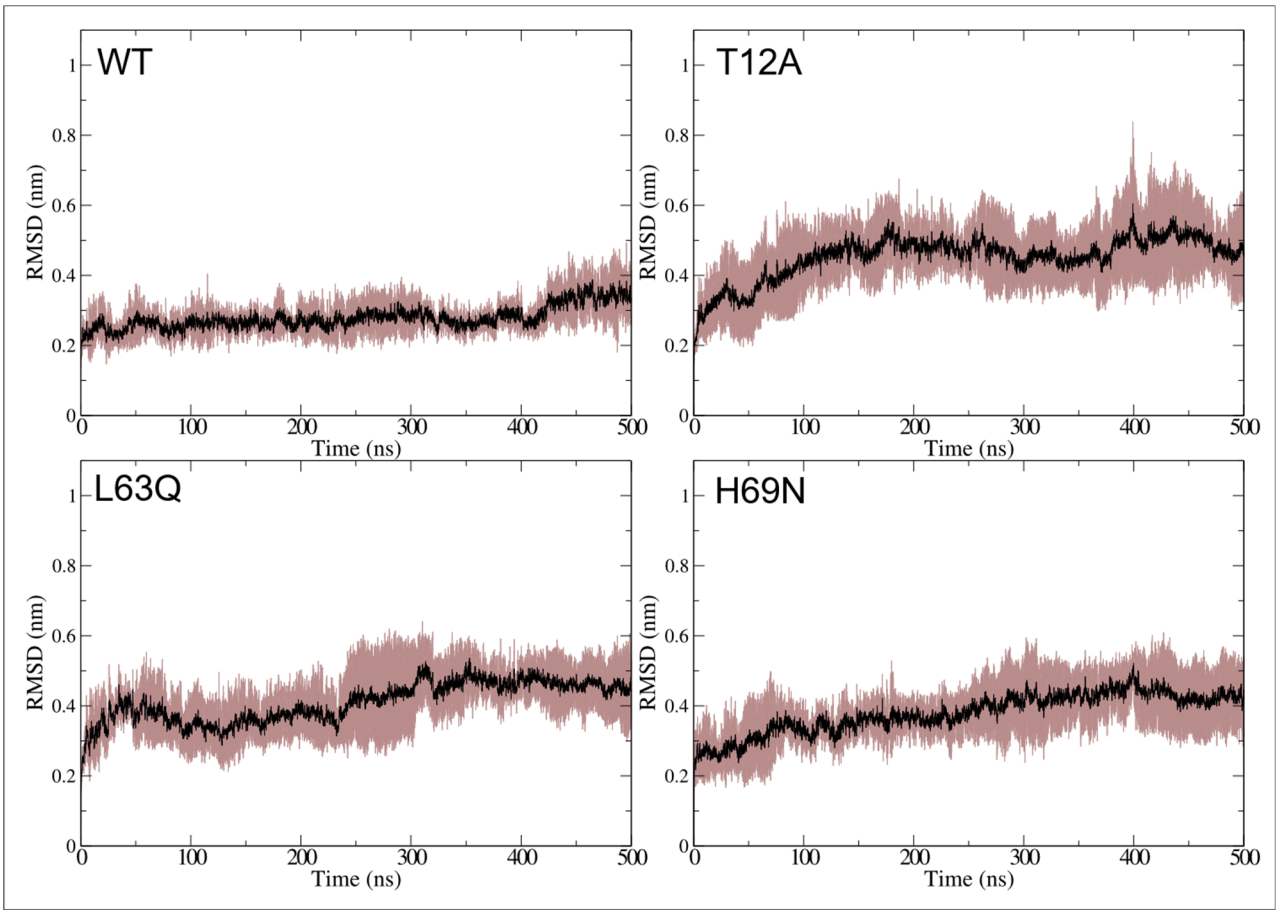

Figure 3. Plot of RMSD of c-alpha atoms with the exclusion of the flap domains residues (43–58), as a function of simulation time for the four simulated PR systems. Average and shaded error range, calculated from the three replicas, are colored in black and brown, respectively.

Table 2. Average and standard deviations RMSD with the exclusion of the flap domains residues (43–58) for native and mutated PR (nm) in the 50–500 ns time window.

		No Flap C-Alpha			
		Ave	**St Dev**	**Max**	**Δ (%)**
Native	R1	0.27	0.03	0.41	−28.95
	R2	0.27	0.04	0.40	−25.00
	R3	0.30	0.05	0.51	−25.00
T12A	R1	0.42	0.03	0.55	−23.64
	R2	0.51	0.11	0.87	−17.74
	R3	0.48	0.07	0.65	−15.79
L63Q	R1	0.39	0.05	0.52	−13.33
	R2	0.46	0.07	0.66	−20.69
	R3	0.39	0.09	0.61	−2.50
H69N	R1	0.43	0.09	0.58	−15.69
	R2	0.41	0.05	0.59	−21.15
	R3	0.33	0.04	0.52	−28.26

As expected, the removal of the flap region leads to a marked reduction in RMSD values in the native system, with average reductions ranging from 25 to 29% across replicas (see Table 2). In the mutants, the reduction is more variable; for example, R3 of L63Q shows only a 2.5% decrease. Notably, even after excluding the flap region, all mutants retain higher RMSD values than the WT, with T12A remaining the most flexible. This indicates that their increased flexibility is not limited to flap motion.

2.2. Protein Flexibility

We next calculated the root-mean-square fluctuation (RMSF) to identify residues whose dynamics are most affected by the mutations. RMSF profiles for the native and mutant systems are shown in Figure 4 as averages with shaded error ranges across replicas, while individual profiles are reported in Supplementary Figure S3.

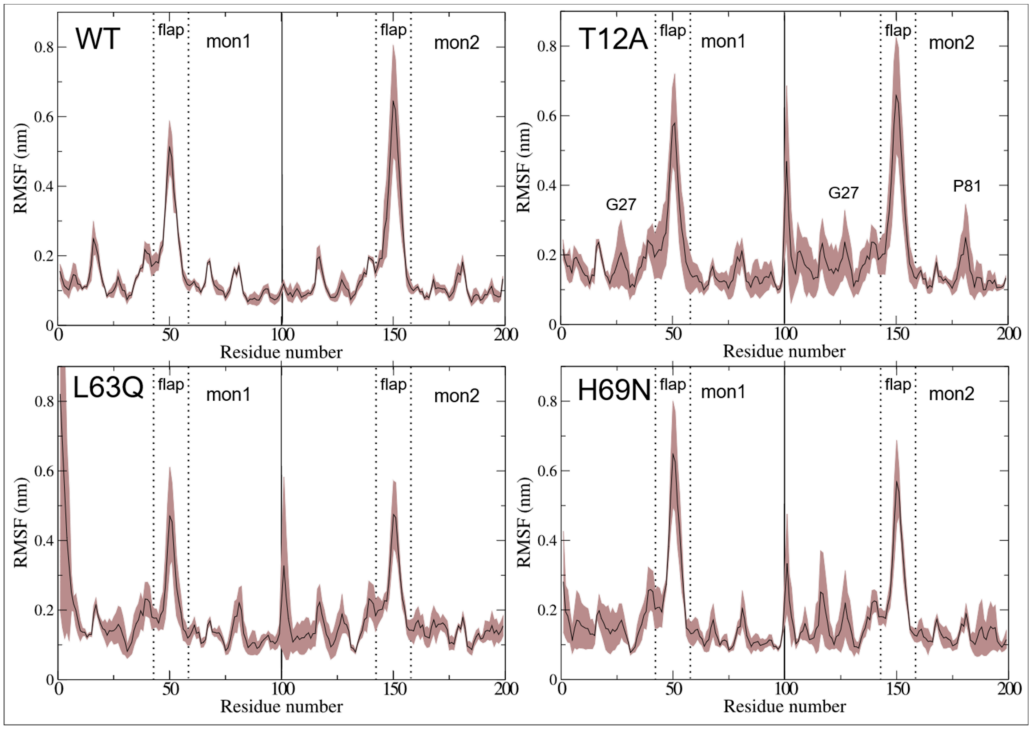

Figure 4. Plot of root-mean-square fluctuations (RMSF) for the two protein chains and the four systems. Average and shaded error range, calculated from the three replicas, are colored in black and brown, respectively.

As expected, the largest fluctuations occur within the flap domains in all systems, across all replicas and both chains. However, notable differences emerge. In the native protein, the two flap domains exhibit asymmetric behavior, with significantly greater fluctuations in chain B than in chain A. In particular, replica R2 (red in Figure S3) shows maximal fluctuations in chain B and minimal fluctuations in chain A compared to R1 and R3 (black and green in Figure S3, respectively). A similar asymmetry is observed in the H69N mutant, although with an inversion between chains: i.e., the R3 replica has maximum fluctuations in chain A and minimum in chain B compared to R1 and R2. In the same system, an important asymmetry of fluctuations is observed also between the two flap domains of R2.

The T12A and L63Q mutations have pronounced but opposite effects. T12A increases flexibility in regions outside the flaps, while flap dynamics remain comparable to WT. This is especially evident in replica R2, where Gly27 (adjacent to the catalytic Asp25) shows enhanced flexibility in both chains (see Figure S3). Additionally, Pro81 in the wall loop

exhibits the highest flexibility outside the flap region in chain B. Conversely, the L63Q mutation exerts a stabilizing effect on global motion of PR, with flap fluctuations never exceeding 0.6 nm in any replica or chain.

2.3. Open Flap Conformation of the HIV-1 PR Systems

The differences between the RMSD with and without the flap region indicate a strong variability in the motion of this region over the 500 ns and across the three replicas. The importance of this region for PR catalytic activity is also evident from the RMSF plots.

For this reason, we calculated the distance between the c-alpha atoms of Ile50 in monomers 1 and 2 as indicator of the open state of the flaps [20–22]. The results show substantial variability in flap opening among replicas and systems. All systems visit open-flap conformations, but only the L63Q mutant does so in less simulation time than the WT, whereas the H69N and T12A distance distributions are shifted toward larger distances, consistent with a higher number of open-flap conformations. Using a 1 nm cut-off, the WT across the three replicas exhibits 65.4% of conformations with distances longer than this threshold, while the corresponding values for L63Q, H69N, and T12A are 55.2%, 82.1%, and 82.6%, respectively. Notably, T12A displays the highest percentage of open-flap conformations, followed by H69N.

To verify that a 500 ns simulation length for the three replicas is sufficient to adequately sample the energy barrier associated with flap opening and closing, we calculated the total number of open–closed and closed–open transitions in each system/replica within the equilibrated 50–450 ns time window. The total numbers are reported in Table 3, considering that all systems started from a closed conformation.

Table 3. Number of transitions between open and closed conformation of the Flaps, and residence time of the open and closed conformation.

		n. Trans	τ_Open (ps)	τ_Closed (ps)
Native	R1	1077	547	289
	R2	2163	272	144
	R3	2829	208	110
T12A	R1	453	1645	345
	R2	1309	568	120
	R3	3293	226	48
L63Q	R1	3333	75	61
	R2	1005	247	201
	R3	883	281	228
H69N	R1	2387	155	34
	R2	509	726	158
	R3	1255	294	64

Residence times (τ) were calculated and are reported in Table 3 (in ps) as the average time spent in each state between consecutive transitions, taking into account the percentage of time spent in the open conformation in each trajectory, following standard kinetic analyses of discrete-state trajectories and Markov state model frameworks [23,24]. Despite the high variability among replicas, all residence times are shorter than 1 ns, except for R1 of T12A, which has a τ in the open conformation of 1.645 ns. Although the calculation of highly accurate residence times is beyond the scope of the present study, we conclude that

a length of 450 ns per replica is sufficient to reliably sample the opening and closing of the PR flaps.

2.4. Secondary Structure

We then compared the secondary-structure content in the four systems. The three simulations show very good reproducibility among the three replicas and conservation of secondary structure throughout the simulations (see Supplementary Figures S4–S15). In Figure 5, we report the secondary-structure occupancy (i.e., the percentage of time spent in a defined secondary structure, averaged over the three simulations). Both native and mutant systems show very good conservation of the alpha-helix around residues 87–95 in both monomers. The nine β-sheets present in each monomer are also conserved over the entire simulation time, with the exception of the four-stranded β-sheet (residues 1–5 and 96–99), which shows reduced structural occupancy only in the three mutants, particularly in L63Q. Notably, the regions harboring the mutations maintain their β-sheet conformation, i.e., the Fulcrum (residues 10–23) in the T12A mutant and the Cantilever (residues 59–75) in the L63Q and H69N mutants. Overall, this analysis indicates that secondary structure remains largely conserved across all variants, and that the observed differences in protein flexibility and flap opening in the mutants are not caused by protein unfolding.

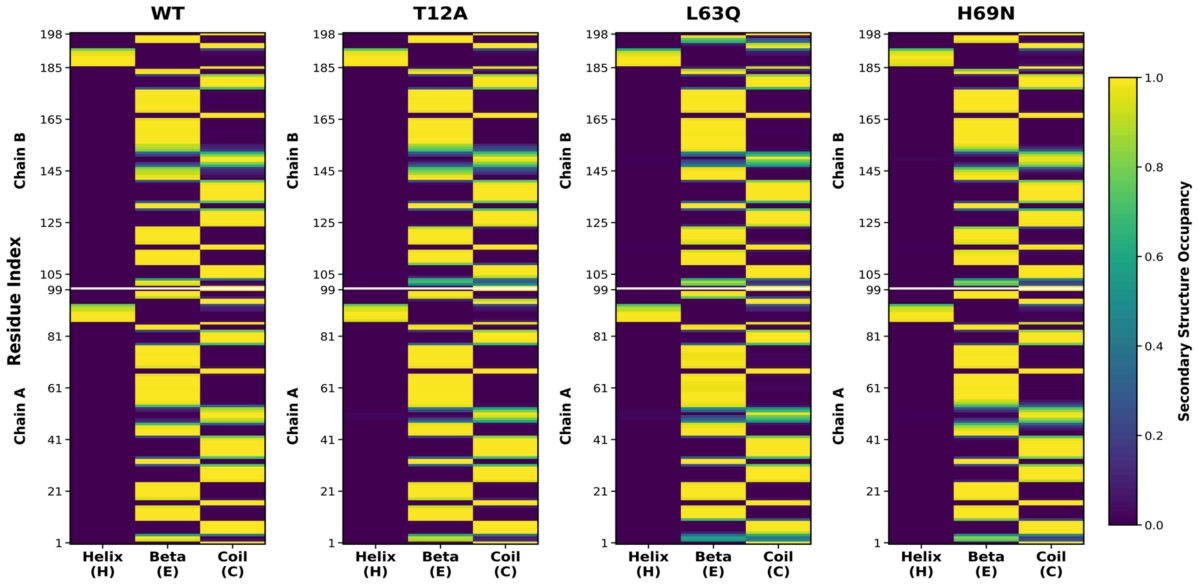

Figure 5. Secondary structure analysis of four systems (WT, T12A, L63Q, and H69N). The plots show residue-wise secondary structure propensities (Helix, β-sheet, and Coil) for chains A and B, averaged over three independent replicas. Colors represent the mean secondary structure occupancy (0–1 scale), highlighting differences in structural stability and local conformational preferences among the variants.

2.5. Hydrogen Bonds of the Mutated and Active Site Residues

We then investigated the local perturbations induced by the mutations by analyzing their stable hydrogen bonds (i.e., present for more than 60% of the simulation time). Mutation of Thr12 to alanine reduces the number of stable hydrogen bonds from six (involving residues Ile13, Lys14, Lys20, Glu21, and Cys67) to only one, between the main chain of Ala12 and Arg8. Conversely, mutation of Leu63 to Gln increases the number of stable hydrogen bonds from one (between the main chains of Leu63 and Gly16) to ten, involving residues Gly16, Gly17, Gln61, Ile64, Glu65, Lys70, and Ala71. The H69N variant shows a hydrogen-bond network more similar to that of the native system. In this case, the number of stable hydrogen bonds increases from six to nine. The residues involved in